The International Journal of Advanced Manufacturing Technology
https://doi.org/10.1007/s00170-024-14090-w

ORIGINAL ARTICLE

An integrated method and tool for telescopic beams design in extendable undercarriages

Luca Catenacci[1] · Pietro Bilancia[2] · Andrea Cavedoni[1] · Marcello Pellicciari[2]

Received: 29 February 2024 / Accepted: 27 June 2024

Abstract
Earth-moving machine builders require innovative design methods and tool to optimize structural performance while reducing production and design costs, particularly in crucial phases like undercarriage frame design and structural verification. After an in-depth description of the design flow normally followed in industry, the paper presents a computationally efficient method and tool to aid designers in dimensioning extendable tracked undercarriages, aiming to drastically reduce design time and efforts to optimize resources. The proposed tool is based on an analytical model established from in-depth analyses of the undercarriage Computer Aided Design (CAD) assembly and the expertise of the industrial partner. To address the 3D structural problem, a planar system is employed with proper corrective coefficients. These coefficients are meticulously evaluated through direct comparison with Finite Element Method (FEM) models by seamlessly integrating SolidWorks and ANSYS Workbench. The tool accepts as inputs geometric and material data, as well as specific user-defined load scenarios, providing outputs in the form of the deflected configuration of the undercarriage and stress levels. Direct comparison with the results obtained from FEM for three industrial undercarriage models demonstrates the validity of the approach, with errors consistently within the 10% range in almost all cases. This enables designers with no advanced skills in FEM to efficiently validate diverse design variants with minimal effort. Once validated, the tool is integrated with an optimizer in Matlab to conduct computationally efficient design optimization studies. The optimization problem, focused on minimizing the beam's vertical size while maintaining structural integrity and limiting deflections, has been successfully resolved within a limited computational time, showcasing the benefits of the proposed approach for undercarriage design.

Keywords Earth-moving machinery · Tracked undercarriage · Engineering design tool · CAD/CAE integration · Structural design

1 Introduction

In the age of Industry 4.0, where the market demands rapid adaptation and the ability to diversify products in response to evolving consumer needs, companies and designers face critical challenges. The constantly evolving market requires companies to diversify their portfolio by configuring a wider array of product variants for customers, strictly designed according to their needs [1]. Achieving a competitive edge necessitates upgrading both design and production phases, maintaining high levels of quality and efficiency. This challenge is particularly relevant in the case of earthmoving machinery, where the intrinsic complexities of components such as tracked undercarriages play a pivotal role [2, 3]. Owing to their superior terrain adaptability and off-road traction performance in comparison to wheeled solutions [4–6], tracked undercarriages have been adopted across various sectors over the last decades [7]. Today, the most competitive constructors are able to deliver highly tailored solutions based on the clients' requests, as shown by [8]. Tracked undercarriages find extensive use not only in construction sites but also in crop production [9] and submarine trenchers [10, 11].

The most critical design phases revolve around the frame embodiment design and its concurrent structural verification to ensure optimal performance, durability, and safety [12–14]. The primary goal is the optimization of the

✉ Pietro Bilancia
pietro.bilancia@unimore.it

[1] Trackone Srl, Via Anton Giulio Barrili, 41123 Modena, Italy

[2] Department of Sciences and Methods for Engineering, Università degli Studi di Modena e Reggio Emilia, via Amendola 2, 42122 Reggio Emilia, Italy

Published online: 09 July 2024

undercarriage mass and vertical size while maximizing strength and robustness to effectively support diverse and cyclic loading scenarios specified by the end-user applications [15, 16]. The complexity arises from the multitude of geometric parameters (a frame is normally composed of hundreds of welded metal sheets) and intricate interactions among parts (e.g. many mutual contacts between different parts characterized by frictional sliding), especially when dealing with extensible undercarriages incorporating additional elements like telescopic beams and hydraulic actuators to adjust the track gauge.

At the industry level, the undercarriage structural design is commonly approached resorting to the Finite Element Method (FEM), enabling accurate analysis of systems with a large number of parts and providing a wide library of modeling features to account for various nonlinearities. Despite these capabilities, 3D FEM (solid elements) may become impractical when several simulations must be performed, as in the case of extensive optimization studies, due to its large computational times [17]. Specifically, a single simulation on an undercarriage made of more than 500 parts (resulting in an overall mesh of 500,000 elements and 400 boundary conditions) can take hours or even days to converge if the nonlinear solvers are activated, while many different design variants are conceived and should be quickly evaluated. From a strategic viewpoint, it is always desirable to rely on accurate and efficient models and tools during the preliminary design phases, i.e. when plenty of design alternatives are to be evaluated, to reduce the overall delays and increase the business competitiveness [18–20]. Furthermore, it is important to note that FEM implementation demands skilled personnel to ensure the proper development and interpretation of models. Despite the growing attention to the performance of earthmoving machinery and related components, as evident from the relevant number of recent research works in the field (see e.g. [13, 21–26]), an accurate and time-efficient behavioral model and tool that supports the undercarriage structural design is missing in the current literature. Therefore, an inefficient iterative empiric approach based on the company know-how is nowadays preferred, usually leading to sub-optimal solutions.

With the aim to overcome the abovementioned limitations, the present paper focuses on the development of an efficient design tool able to quickly calculate the bending deformation and stress state of extendable undercarriages under various combinations of input geometric parameters and loading conditions. After a meticulous analysis of the loads exerted on the undercarriage during operation, emphasis has been placed on the front axle, which is the most loaded sub-assembly. This is modeled resorting to the Euler–Bernoulli's beam theory as a system of three beams representing the right/left tubular elements and the central body. To obtain the moment of inertia of the central body, characterized by a nonstandard geometric shape, an integrated Computer Aided Design/Engineering (CAD/CAE) framework that incorporates SolidWorks and ANSYS Workbench is defined. The evaluation process involves assessing the influence of the main parameters through dynamic updates to the geometry and subsequent FEM verification (see Refs. [27–31] for more details). At last, the proposed theoretical model is analytically solved, and the derived formulas are incorporated into a calculation tool to favor its easy and efficient use in industry. In this way, the designer can keep the focus on inventing novel design solutions, which are quickly validated and dimensioned with the tool, drastically reducing time and efforts.

The remaining of the paper is organized as follows. Section 2 describes the undercarriages main features and details its industrial design method. Section 3 reports about the undercarriage static modeling. Section 4 details the model FEM validation and its subsequent integration into an interactive design tool, which is then integrated with an optimizer to perform size optimization on an industrial test case. The concluding remarks are given in Section 5.

2 Undercarriage design overview

2.1 System description

The undercarriage constitutes the lower section of an earthmoving machine, as shown in Fig. 1. During operation, it constantly withstands both the weight of the upper machine, including all the components and subsystems that define the machine utilization (e.g. drilling mast for a drilling machine) and the heavy working loads arising from the specific operational cycle. Furthermore, the undercarriage plays a crucial role in managing the machine locomotion. This study specifically focuses on tracked systems, namely systems employing continuous tracks (series of interconnected metal links joined by pins) to generate the desired movement.

Undercarriages are typically composed by a welded steel frame and many track components, which can be identified from Fig. 1 as follows (see also [32] for more details):

- Track chain, consisting of a series of chain links and track shoes connected by bush-pin couplings.
- Track rollers, which support the weight of the machine and slide on the planar side of the chain link.
- Sprocket, i.e. the driving wheel that engages with the track chain to provide the traction force.
- Idler, which is the front wheel of the undercarriage whose function is to guide the chain. It usually comes coupled with a spring unit, made up of a shock absorber and a tensioner, which it used to set the correct preload for the track chain.

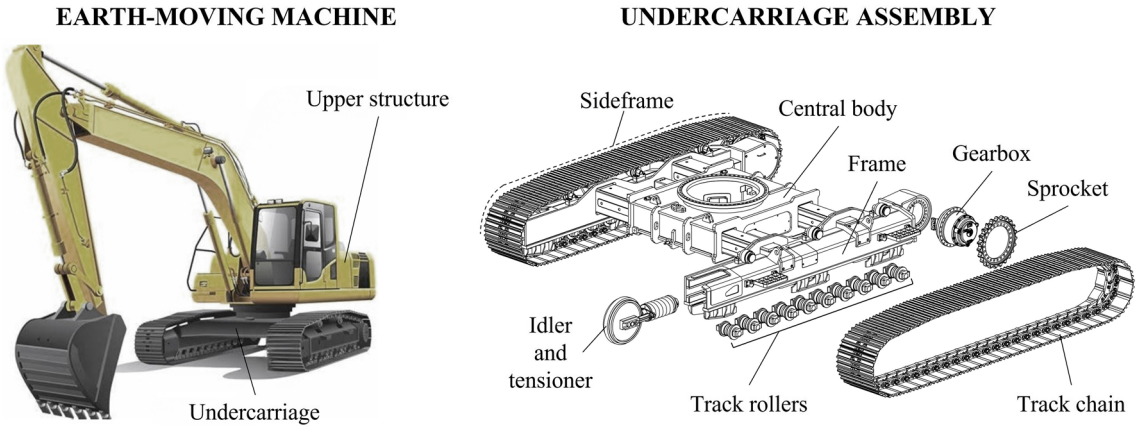

Fig. 1 Undercarriage components view

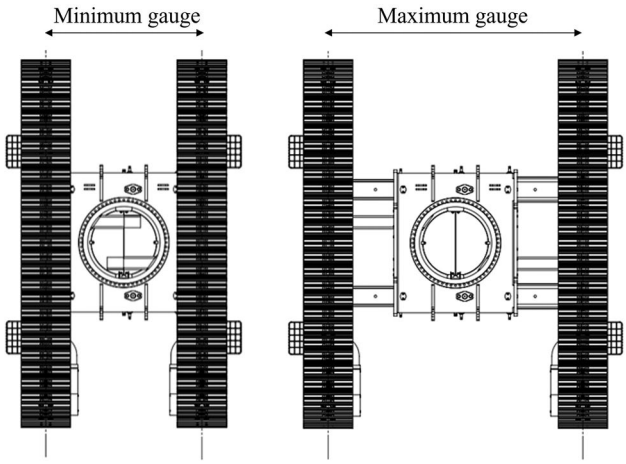

Fig. 2 Gauge-varying in extendable undercarriages: minimum Vs. maximum opening

As it can be seen, tracks, rollers, idlers, and other associated mechanisms are housed in the sideframe on both sides of the undercarriage. The most intricate and time-intensive undercarriages, concerning product development, costs, and production, are the extendable ones. These formats offer the flexibility to vary the track gauge, resulting in two distinct configurations: minimum and maximum opening (see Fig. 2). The transition between configurations provides the following advantages:

1. greater stability during work in the fully open track configuration;
2. reduced overall dimensions in the minimum track configuration, ensuring compliance with dimensional limits for exceptional transports on trucks.

In the case of extendable undercarriages, additional components, including extension beams and a welded metal structure housing the telescopic beams (referred to as the central body in Fig. 1), need to be taken into account. These beams not only slide into each other but also within the housing of the central body. This configuration results in numerous frictional contacts and connections in the central area, where also stress concentrations take effect. These factors make the prediction of the structural behavior of this zone a complex task.

2.2 Design process

The flow typically adopted in industry for the design of a newly commissioned undercarriage consists of many sequential steps, as highlighted in Fig. 3.

In particular, three main phases can be identified [33]:

- **Preliminary design**, covering the requirements gathering, technical specification definition, planning, risk analysis, up to the definition of a preliminary layout and its subsequent quotation.
- **Detailed design**, characterized by the maximum company resources usage as both the embodiment CAD design and the Computer Aided Engineering (CAE) verifications can take several weeks.
- **Check and refinement**, where the last details are completed before ending with the final documentation and the production.

As it can be noted from Fig. 3, behavioral modeling and simulation are predominantly conducted during the second phase of the process [34]. In particular, the undercarriage sizing primarily involves static FEM analyses, with load scenarios provided directly by the end-user. The loads

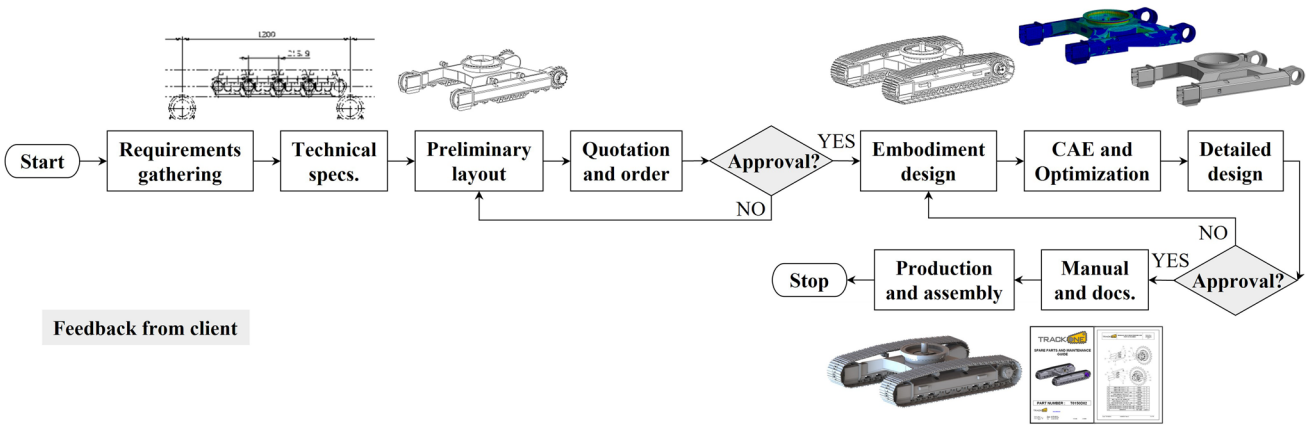

Fig. 3 Undercarriage design workflow

transmitted to the undercarriage comprise various contributions (e.g. upper machine weight, working conditions, payload, etc.) as illustrated in Fig. 4. However, as previously mentioned, FEM proves to be demanding and time-consuming due to the large number of parts (even with non-fine mesh options, i.e. free second-order tetrahedral mesh with 15 mm as the element size), connections, and boundary conditions required in the models. Consequently, running optimization studies with many possible iterations would lead to high computational times (the reader should refer to [17] for further insights and [35–37] for practical applications). From a strategic perspective, the following points may need careful attention in order to enhance the efficiency and effectiveness of the undercarriage design process:

1. It is advisable to address structural assessments even in the preliminary design phase. This would aim to reduce overall project timelines by having more relevant data early on, facilitating the estimation of the product dimensions and providing valuable information for precisely quoting the undercarriage to the client.
2. The sizing should be conducted without relying on FEM. Given the need to quickly assess various design candidates, computationally efficient methods and tools should

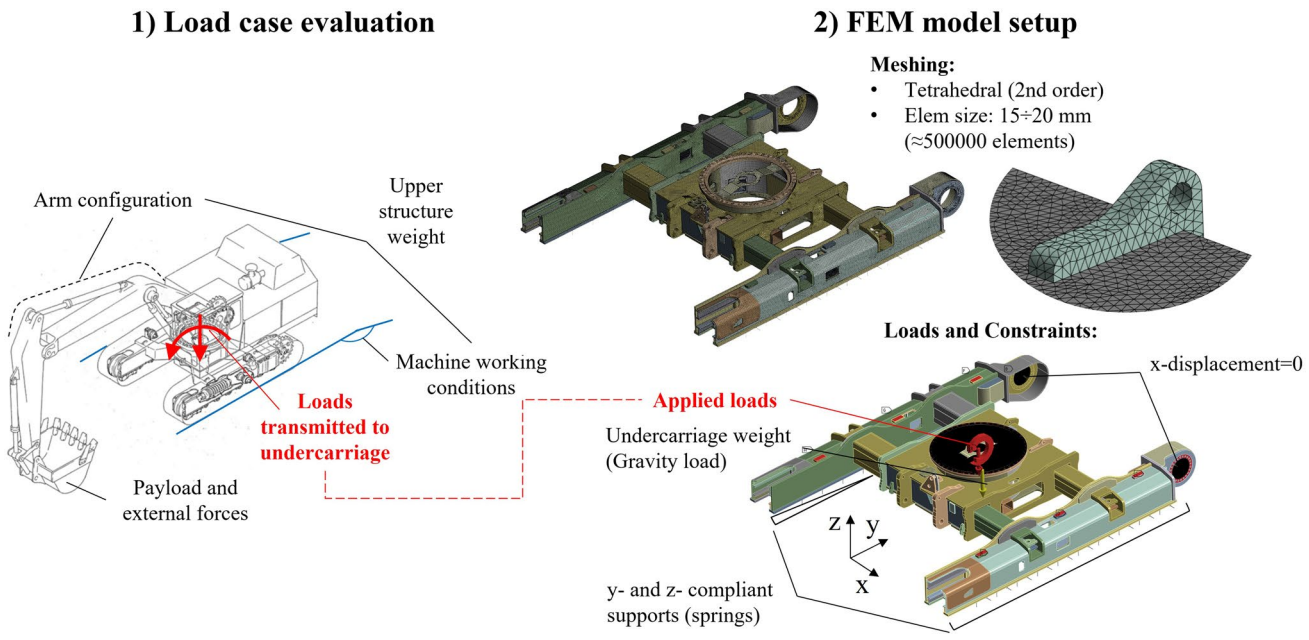

Fig. 4 Loads acting on the undercarriage and related FEM model

be preferred, reserving the use of FEM for the next stages, namely for few detailed analyses and final checks.
3. Manufacturing design guidelines should be implemented to deploy feasible and cost-effective solutions.

Building upon these considerations, in the following sections an efficient and easy-to-use calculation tool able to quickly return an estimation of the undercarriage deformed shape and maximum bending stress is developed and validated on various commercial undercarriage models from the industrial partner and specific load cases. The tool is based on a simplified yet efficient analytical model which can be easily tuned based on the design specifications.

3 Static modeling

As the main target is to develop a fast and accurate design tool, a geometry analysis is needed to delineate and schematize the structural problem, so that it can be modeled and solved adopting well-established theories of structural mechanics. Leveraging the company expertise and incorporating insights from preliminary FEM simulations, in this analysis particular emphasis is placed on the front axle, namely the most critical area, where the maximum stresses and deformation happen in the telescopic beams and in their housings. This hypothesis can be easily verified by checking the longitudinal load distribution on the track rollers in Fig. 5, obtained by plotting the reaction forces on a FEM model subject to a standard load case where the external load originated from the upper machine is positioned in front of the undercarriage. Specifically, the asymmetrical distribution underlines that the majority of the transmitted load are exerted on the front axle, which will be therefore deeply analyzed in the remaining of this work.

3.1 CAD-based analysis and model definition

From a closer examination of the front axle sub-assembly CAD model and, in particular, of its section view reported in Fig. 6, the following considerations are made:

- Three main structural entities are identified, hereinafter named inner beam, outer beam, and central body.
- Points 1 and 5 represent the frame contact points with the ground. Here the entire weight of the upper machine is supported by the track rollers and chain links (see the enlarged view in Fig. 7).
- Points 2 and 4 indicate the telescopic beams entrance area in the central body.
- Point 6 represent the contact point between the outer beam and the central body.
- Points 3 and 7 are the extremities of the beams overlapping portion.

Although points 6 and 7 coincide spatially (see Fig. 6), they refer to different aspects in the context of this structural problem. Point 6 describes the interaction between the outer beam (in red) and the central body (in gray), whereas point 7 focuses on the interaction between the outer beam and the inner beam (in blue). Also, such points do not rely on the vertical middle axis for all the undercarriages models. Naturally, the undercarriage configuration in its fully extended state, characterized by minimal geometric overlap (let us compare Figs. 2 and 6), will exhibit the highest deflections and therefore represents the most studied configuration.

As for the boundary conditions considered in the model, namely the connections among the structural entities and the imposed constraints set, the following observations hold:

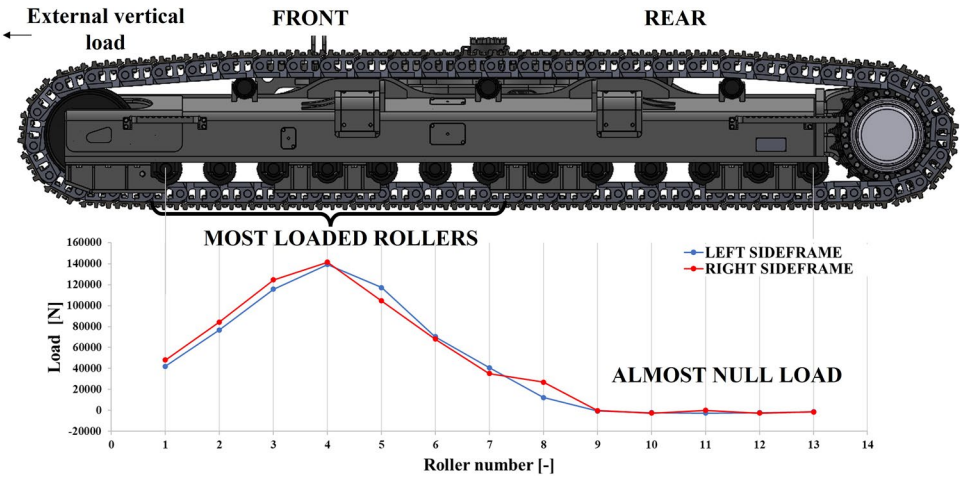

Fig. 5 Rollers load distribution in case of purely front external load

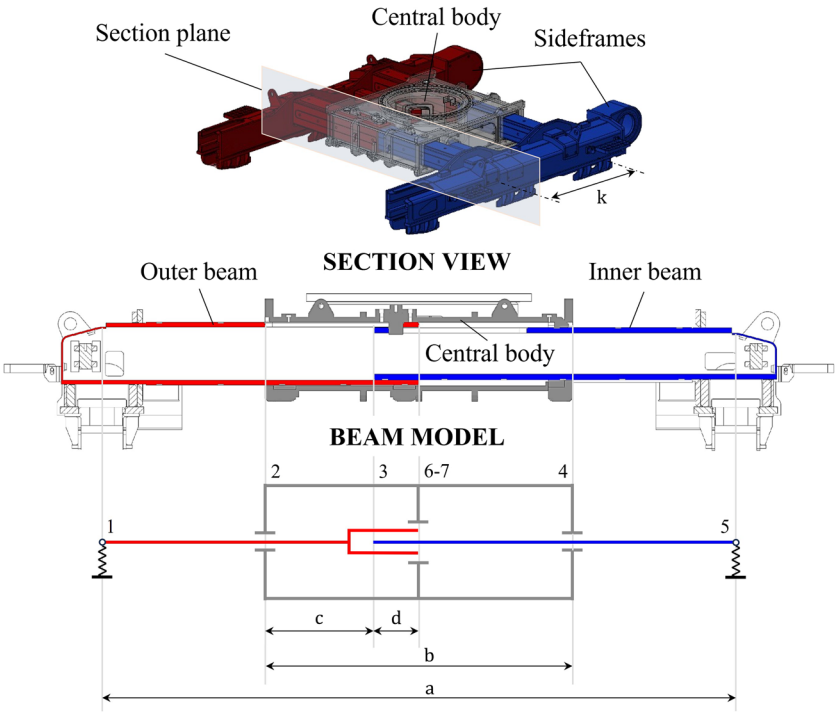

Fig. 6 Section view of the front axle CAD drawing and obtained structural schematic. In the picture, a is the total track gauge, b is the central body width, c is the distance between the end of the inner beam and the extremity of the central body, d identifies the overlapping length, and k is the central body length

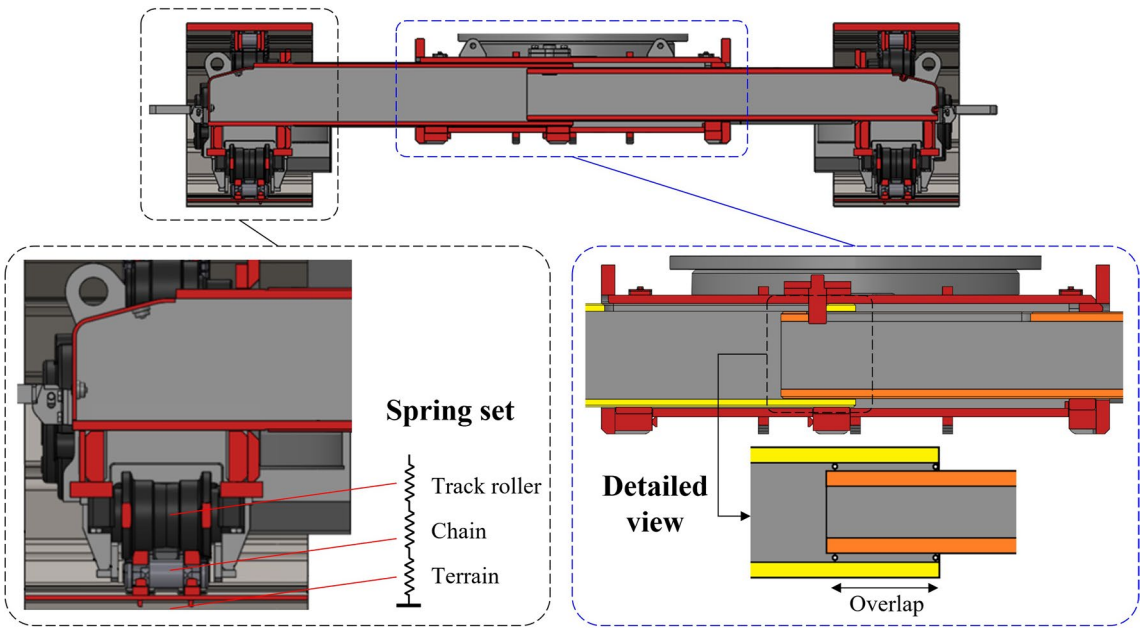

Fig. 7 Ground contact point detailed view

1. **Revolute joints at extremities** (points 1 and 5): by analyzing the connection at the beams extremities shown in Fig. 7, it is evident that the track roller is solely supported and in contact with the chain link (i.e. no bolted connections). Consequently, the track roller is free to rotate by pivoting on the extremal area of the roller crest, allowing the rotation of the entire frame.
2. **Spring connections at extremities** (points 1 and 5): the undercarriage moves on different terrains, from soft sand to asphalt or concrete. Therefore, to account for the terrain stiffness in the model, the above discussed revolute joint is characterized by a certain vertical compliance, defined by a spring constant. Such constant is given by three different contributions in series: the track roller

stiffness, the chain stiffness, and the terrain stiffness. However, in the calculation of the equivalent spring stiffness (K_{eq}), the terrain contribution dominates being far lower than the others. By combining the company know-how and the results of previous studies, K_{eq} has been set equal to 445,000 N/mm for earthy soils and equal to 800,000 N/mm for harder soils (e.g. rocks or asphalt). With reference to Fig. 5, a specific number, denoted as n_r, of track rollers working in parallel is being considered at both supports.

3. **Couplings with central body** (points 2, 4, and 6): the contact areas between the beams and the central body vary according to the presence of recovery wedges and anti-wear plates, used to recover the assembly gap, as shown in Fig. 7. Consequently, the beams are usually not in contact with the central body along their entire length, and the sliding takes place only in the areas where the space between the beams and the central body is absent. Being the beams not strictly fitting the central body housing, the sliding surfaces are not modeled as a prismatic coupling, but rather as simple sliding supports. In fact, the prismatic joint would imply not only a support reaction force but also a reaction moment, which cannot be present since the sliding area is very small and, despite the presence of recovering wedge/plates, there is some remaining vertical clearance that allows the rotation of the beams with respect to the central body.
4. **Coupling between beams** (from point 3 to 7): to keep the model as simple as possible without losing accuracy and reliability, the beams overlap has been modeled as a couple of simple sliding supports: the contacts happen punctually at the end surfaces of the overlap region.

It is important to note that, in this model, all sliding supports have been assumed to be frictionless, as frictional have a minimal impact on the overall vertical deformation of the model.

3.2 Applied loads

Depending on the application of the earth-moving machine, the undercarriage is subject to different external loads, including both the upper machine weight and its operational loads. As illustrated in Fig. 8, the machine self-weight may not be centered on the undercarriage center of gravity. This can occur due to variations in machine configurations, as seen in drilling operations where the drilling mast may be raised to bore holes or kept lowered during locomotion phases. Additionally, the upper machine turret has the capability to fully rotate on the swivel bearing, allowing working loads to be applied from any direction around the machine (described by angle α).

Due to the above considerations, the undercarriage experiences not only a vertical force but also a moment at the swivel bearing, where the upper machine connects to the frame. The customer typically provides to the company the total vertical load F_t, applied in the center of a reference system Oxyz (where O coincides with the undercarriage center of gravity), and the maximum moment M_t, which can manifest at any working load angle α. Since the maximum stresses occur in the telescopic beams, the specified force and moment are decomposed to analyze their effects on the front axle. In this process, the initial 3D load case is transformed into applicable conditions for the schematized 2D model, as shown in Fig. 9. In particular, the moment M_t is decomposed in its components M_{tx} and M_{ty}, whose magnitude will depend by the working angle α. M_{ty} can be further decomposed in its generatrix forces, dividing the moment by its arm, that is the central body length k. Concerning the vertical load F_t and the moment M_{tx}, these are simply divided by 2 and moved to the front and rear axles.

While performing these force transfers, torsional moments acting on the front and rear axles should also be added to the model. However, based on the company's

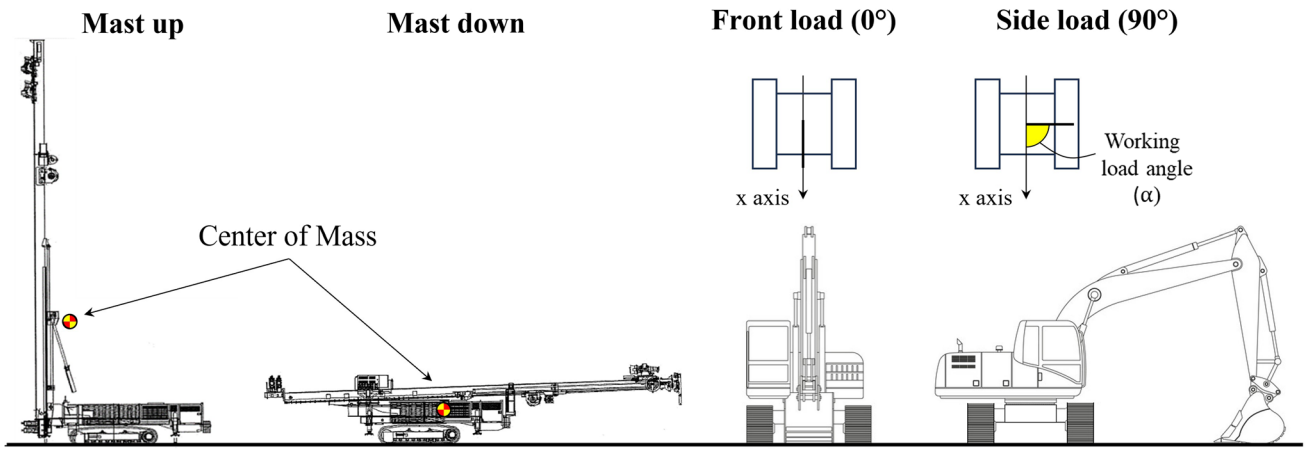

Fig. 8 Center of gravity and working load conditions for a generic undercarriage

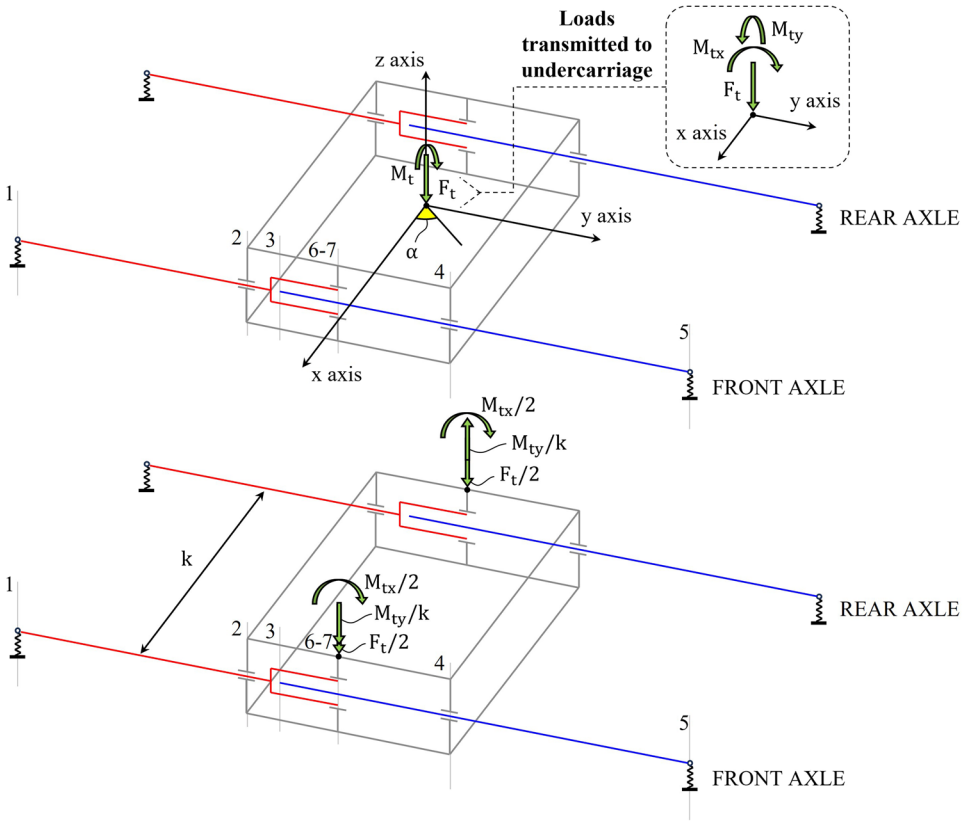

Fig. 9 External loads applied on the schematized structure

know-how and common engineering practice, it is essential to highlight that these effects are consistently at least one order of magnitude lower than the considered flexural contributions. Therefore, given that the developed model is aimed at defining an easy-to-use and rapid tool to predict the undercarriage structural behavior, the influence of torsional moments has been disregarded.

Another significant contribution is the undercarriage self-weight, denoted as F_w, which is usually about 10–20% of the total vertical load and, therefore, cannot be neglected in the calculations. As said, the undercarriage comprises numerous components, and considering that distributed loads would introduce unnecessary complications in the model, the weights are merged in three main groups and applied at specific points. In particular, contributions from the sideframes (each approximately $F_w/3$) are applied at points 1 and 5, whereas the central body contribution, inclusive of the beams weight and equaling $F_w/3$, is applied at the midpoint, as shown in Fig. 10.

3.3 Theoretical formulation

The geometry and load analysis outlined in Section 3.1-3.2 lead to the structural problem depicted in Fig. 10, which can be solved with the Euler–Bernoulli linearized beam theory under the assumption of small deflections [38]. In particular, the governing equation is as follows:

$$U_z''(s) = \frac{M_x(s)}{EJ(s)} \tag{1}$$

where U_z, M_x, and J are respectively the beam vertical displacement, bending moment, and cross-section moment of inertia expressed as functions of the coordinate s (depicted in Fig. 10), whereas E represents the material elastic modulus. To simplify the model setup and resolution, the three beams have been divided into the following segments:

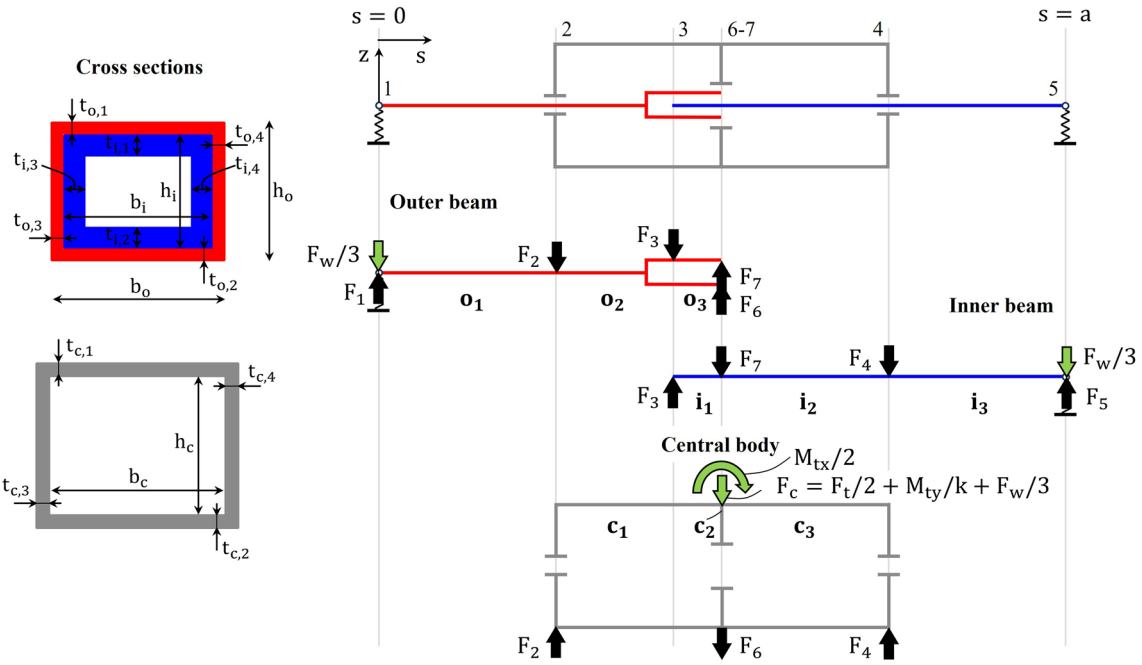

Fig. 10 Front axle loads scheme. The external forces are shown in green and are applied at the extremities and at midpoint. The reaction forces are shown in black. F_1 and F_5 are the reaction force at the yielding hinge constraints; F_2, F_4, and F_6 are the contact forces related to the central body and beams contacts; F_3 and F_7 are the telescopic beam contact forces in the overlap region

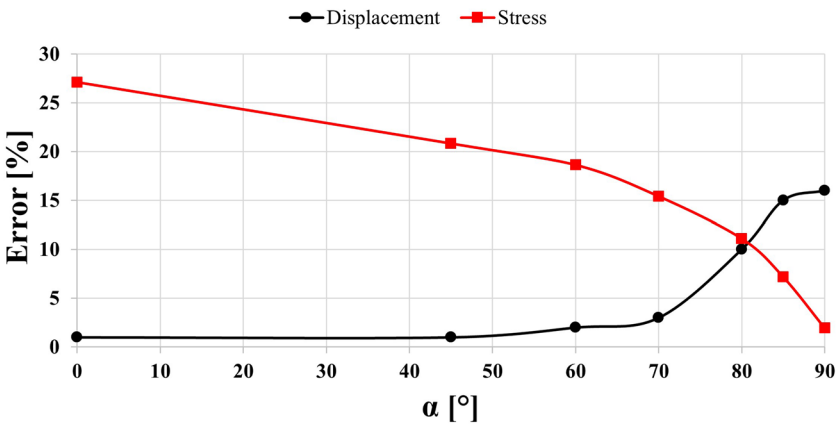

Fig. 11 Percentage α-dependent errors in displacements and stress between FEM and analytical models

- Outer (red) beam $\rightarrow$
$$\begin{cases} segment\ \mathbf{o}_1(\text{point } 1 \rightarrow \text{point } 2) : 0 \le s \le (a-b)/2 \\ segment\ \mathbf{o}_2(\text{point } 2 \rightarrow \text{point } 3) : (a-b)/2 \le s \le (a-b)/2 + c \\ segment\ \mathbf{o}_3(\text{point } 3 \rightarrow \text{point } 7) : (a-b)/2 + c \le s \le (a-b)/2 + c + d \end{cases}$$
- Inner (blue) beam $\rightarrow$
$$\begin{cases} segment\ \mathbf{i}_1(\text{point } 3 \rightarrow \text{point } 7) : (a-b)/2 + c \le s \le (a-b)/2 + c + d \\ segment\ \mathbf{i}_2(\text{point } 7 \rightarrow \text{point } 4) : (a-b)/2 + c + d \le s \le (a+b)/2 \\ segment\ \mathbf{i}_3(\text{point } 4 \rightarrow \text{point } 5) : (a+b)/2 \le s \le a \end{cases}$$
- Central body $\rightarrow$
$$\begin{cases} segment\ \mathbf{c}_1(\text{point } 2 \rightarrow \text{point } 6) : (a-b)/2 \le s \le (a-b)/2 + c + d \\ segment\ \mathbf{c}_2(\text{point } 6 \rightarrow \text{midpoint}) : (a-b)/2 + c + d \le s \le a/2 \\ segment\ \mathbf{c}_3(\text{midpoint} \rightarrow \text{point } 4) : a/2 \le s \le (a+b)/2 \end{cases}$$

Such approach has led to redefining Eq. 1 for each of the nine segments. In particular, the bending moment function can be written as

$$M_{x,o1} = \left(F_1 - \frac{F_W}{3}\right)s \tag{2}$$

$$M_{x,o2} = M_{x,o1} - F_2\left(s - \frac{a-b}{2}\right) \tag{3}$$

$$M_{x,o3} = M_{x,o2} - F_3\left(s - \frac{a-b}{2} - c\right) \tag{4}$$

$$M_{x,i1} = F_3\left(s - \frac{a-b}{2} - c\right) \tag{5}$$

$$M_{x,i2} = M_{x,i1} - F_7\left(s - \frac{a-b}{2} - c - d\right) \tag{6}$$

$$M_{x,i3} = M_{x,i2} - F_4\left(s - \frac{a+b}{2}\right) \tag{7}$$

$$M_{x,c1} = F_2\left(s - \frac{a-b}{2}\right) \tag{8}$$

$$M_{x,c2} = M_{x,c1} - F_6\left(s - \frac{a-b}{2} - c - d\right) \tag{9}$$

$$M_{x,c3} = M_{x,c2} - F_c\left(s - \frac{a}{2}\right) + \frac{M_{tx}}{2} \tag{10}$$

where $F_1, \ldots, F_7$ are the reaction forces, F_w, F_c, and M_{tx} are the external forces (as explained in Section 3.2 and recalled in Fig. 10), whereas a, b, c, and d are the geometric distances as shown in Fig. 6. In the same manner, the moment of inertia is calculated for each segment approximating them as box-shaped bodies with constant cross section along the length. Since the beams and the central body could be made of different metal sheets, the required input data are not only the width and height of the section, but also the four metal sheets thicknesses values. Therefore, the resulting formulas for the outer boxed beam (J_o), inner boxed beam (J_i), and central body (J_c) become

$$J_o = \frac{1}{12}\left(b_o h_o^3 - \left(b_o - t_{o,3} - t_{o,4}\right)\left(h_o - t_{o,1} - t_{o,2}\right)^3\right) \tag{11}$$

$$J_i = \frac{1}{12}\left(b_i h_i^3 - \left(b_i - t_{i,3} - t_{i,4}\right)\left(h_i - t_{i,1} - t_{i,2}\right)^3\right) \tag{12}$$

$$J_c = \frac{1}{12}\left(\left(b_c + t_{c,3} + t_{c,4}\right)\left(h_c + t_{c,1} + t_{c,2}\right)^3 - b_c {h_c}^3\right) \tag{13}$$

where b and h are respectively the total width and height of the boxed beams, whereas t_1, t_2, t_3, and t_4 represent the thicknesses of the upper, lower, left, and right metal sheets within the specific segment (being subscripts "o", "c", and "i" used to indicate the three different beams, as visible in Fig. 10). Considering that approximating complex bodies as a simple boxed section determines a certain amount of error in the results, specific corrective coefficients will be evaluated in Section 3.4.

Once all the necessary relationships are established, the vertical displacement function, U_z, can be determined for each segment by performing a double integration of Eq. 1, leading to the following expressions:

$$U_{z,o1} = C_2 - \frac{1}{18EJ_o}\left((F_W - 3F_1)s^3 - 18C_1EJ_o s\right) \tag{14}$$

$$U_{z,o2} = C_4 - \frac{1}{36EJ_o}\left((2F_W + 6F_2 - 6F_1)s^3 + (9F_2 b - 9F_2 a)s^2 - 36C_3EJ_o s\right) \tag{15}$$

$$U_{z,o3} = C_6 - \frac{1}{36EJ_o}\left((2F_W + 6F_3 + 6F_2 - 6F_1)s^3 + (-18F_3 c + \left(9F_3 + 9F_2\right)b - (9F_3 + 9F_2)a)s^2 - 36C_5EJ_o s\right) \tag{16}$$

$$U_{z,i1} = C_8 + \frac{1}{12EJ_i}\left(2F_3 s^3 + (-6F_3 c + 3F_3 b - 3F_3 a)s^2 + 12C_7EJ_i s\right) \tag{17}$$

$$U_{z,i2} = C_{10} - \frac{1}{12EJ_i}\left((2F_7 - 2F_3)s^3 + (-6F_7 d + (6F_3 - 6F_7)c + (3F_7 - 3F_3)b + (3F_3 - 3F_7)a)s^2 - 12C_9EJ_i s\right) \tag{18}$$

$$U_{z,i3} = C_{12} - \frac{1}{12EJ_i}\left((2F_7 + 2F_4 - 2F_3)s^3 + (-6F_7 d + (6F_3 - 6F_7)c + (3F_7 - 3F_4 - 3F_3)b + (-3F_7 - 3F_4 + 3F_3)a)s^2 - 12C_{11}EJ_i s\right) \tag{19}$$

$$U_{z,c1} = C_{14} + \frac{1}{12EJ_c}\left(2F_2 s^3 + (3F_2 b - 3F_2 a)s^2 + 12C_{13}EJ_c s\right) \tag{20}$$

$$U_{z,c2} = C_{16} - \frac{1}{12EJ_c}\left((2F_6 - 2F_2)s^3 + (-6F_6 d - 6F_6 c + (3F_6 - 3F_2)b + (3F_2 - 3F_6)a)s^2 - 12C_{15}EJ_c s\right) \tag{21}$$

$$U_{z,c3} = C_{18} - \frac{1}{12EJ_c}\left((2F_c + 2F_6 - 2F_2)s^3 + (-6F_6 d - 6F_6 c + (3F_6 - 3F_2)b + (-3F_c - 3F_6 + 3F_2)a - 3M_{tx})s^2 - 12C_{17}EJ_c s\right) \tag{22}$$

Here $C_1, \ldots, C_{18}$ are the integration constants (2 for each differential equation). Considering also the presence of the reaction forces $F_1, \ldots, F_7$, the total number of unknowns to be determined is 25. To solve the mathematical problem, the following additional relations expressing the congruence among displacements must be incorporated:

at point 1, $s = 0$: $U_{z,o1} = -F_1/n_r K_{eq}$ (23)

at point 2, $s = \frac{a-b}{2}$:
$U_{z,o1} = U_{z,o2}$ (24)
$U'_{z,o1} = U'_{z,o2}$ (25)
$U_{z,o2} = U_{z,c1}$ (26)

at point 3, $s = \frac{a-b}{2} + c$:
$U_{z,o2} = U_{z,o3}$ (27)
$U'_{z,o2} = U'_{z,o3}$ (28)
$U_{z,o3} = U_{z,i1}$ (29)
$U_{z,c2} = U_{z,c1}$ (30)
$U'_{z,c2} = U'_{z,c1}$ (31)

at points 6 − 7, $s = \frac{a-b}{2} + c + d$:
$U_{z,o3} = U_{z,i1}$ (32)
$U_{z,o3} = U_{z,c2}$ (33)
$U_{z,i2} = U_{z,i1}$ (34)
$U'_{z,i2} = U'_{z,i1}$ (35)

At midpoint, $s = \frac{a}{2}$:
$U_{z,c3} = U_{z,c2}$ (36)
$U'_{z,c3} = U'_{z,c2}$ (37)

at point 4, $s = \frac{a+b}{2}$:
$U_{z,i3} = U_{z,i2}$ (38)
$U'_{z,i3} = U'_{z,i2}$ (39)
$U_{z,i3} = U_{z,c3}$ (40)

at point 5, $s = a$: $U_{z,i3} = -F_5/n_r K_{eq}$ (41)

Also, the vertical force equilibrium is imposed for the three beams, i.e.:

Outer beam $F_1 - F_2 - F_3 + F_6 + F_7 - \frac{F_w}{3} = 0$ (42)

Inner beam $F_3 - F_7 - F_4 + F_5 - \frac{F_w}{3} = 0$ (43)

Central body $F_2 - F_6 + F_4 - F_c = 0$ (44)

At last, the following expressions are added to impose the null moment at the right extremity of each beam:

Outer beam, $s = \frac{a-b}{2} + c + d$: $M_{x,o3} = 0$ (45)

Inner beam, $s = a$: $M_{x,i3} = 0$ (46)

Central body, $s = \frac{a+b}{2}$: $M_{x,c3} = 0$ (47)

The model has been analytically solved in Matlab, employing the symbolic math toolbox to derive practical formulas. The primary outputs include the beam vertical displacement $U_z(s)$, which is plotted in the range s ∈ [0, a] to visualize the deformed shape, and the bending stress, calculated as follows [38]:

$$\sigma_b(s) = \frac{M_x(s)h/2}{J(s)} \tag{48}$$

To take into consideration any secondary effect or approximation made in the previous sections, the model incorporates corrective coefficients for $U_z(s)$ and $\sigma_b(s)$, which will be introduced in the remainder of this section.

3.4 Corrective coefficients evaluation

Preliminary comparisons with FEM data obtained from different undercarriages models have shown deviations in the analytical results. In particular, both vertical displacements and stresses have been compared by extracting probe data from ANSYS Workbench. Vertical (z-)displacements are assessed by considering the nodes located on the neutral axis of the beams of the front axle, whereas the Von Mises stresses are obtained by exporting the stress probes from the most critical bending regions, specifically where the beams enter the central body. The observed differences between FEM and theoretical results (reaching up to 20% at this stage) are mainly

due to the simplifications introduced during the calculation of J_c using a simplified formula for boxed beams. Notably, the central body does not present a beam-like geometry, and its structural properties are influenced by various geometric parameters. Moreover, as visible in Fig. 11, comparisons made considering different load scenarios have highlighted a dependency of the errors from the angle α, i.e.:

- **Displacements**: error is limited when α is up to 45°, then started to rise reaching the maximum at 90° (purely lateral load). This behavior can be justified by the simplifications introduced during the geometric and load modeling of the structural problem, i.e. when the original loads are decomposed to obtain forces and moments acting on the front axle of the undercarriage and the 3D geometry is simplified to a 2D beam-like structure (see Figs. 9 and 10).
- **Stresses**: error reaches its maximum at 0° (purely frontal load), but is considerably limited at around 90°. This is attributed to the lack of marked additional stress components (e.g. torsional, local effects) when the load is on the beam plane (i.e. for $\alpha = 90°$).

Due to the above reasons and with the objective of enhancing the accuracy of the analytical model, the following corrections are implemented. Two coefficients, namely $\mu_1(\alpha)$ and $\mu_2(\alpha)$, corresponding to displacements and stresses, are derived through careful mathematical fitting of the results presented in Fig. 11. Such coefficients are expressed as follows:

$$\mu_1 = 1 + 0.16\,(sen\ \alpha)^{32} \quad \mu_2 = 1/\left(1.05 + 0.25\,(cos\ \alpha)^{\frac{5}{4}}\right) \tag{49}$$

and are applied to the previous functions $U_z(s)$ and $\sigma_b(s)$ for $s \in [0, a]$:

$$U_{z,corr} = \mu_1 U_z \quad \sigma_{b,corr} = \mu_2 \sigma_b \tag{50}$$

to correct for any possible load case.

Subsequently, a corrective factor to account for the stiffness characteristics of the central body (not included in the earlier formula for J_c expressed in Eq. 13) is introduced. The coefficient is determined through a parametric study conducted in an integrated CAD/CAE environment [39]. In fact, the undercarriage welded frame presents a highly non-standardized geometry, consisting of multiple reinforcement plates of varying thickness arranged to form a specific shape. Thefore, the use of a CAD tool is imperative to capture all these effects accurately. Then, to fully exploit the simulation capabilities of commercial FEM solvers, a framework integrating SolidWorks and ANSYS Workbench has been established by connecting their workspaces, as detailed in [17, 27, 28]. This enables the creation of a parametric CAD model that is iteratively updated and seamlessly transferred into the ANSYS structural environment, as shown in Fig. 12. In this environment, loads and constraints are applied before initiating the i-th analysis automatically. For the parametric study, a simplified CAD model of the undercarriage is created. This model is conceived to allow easy modification by varying few key dimensions (i.e. the considered parameters). Therefore, it excludes non-essential elements for mechanical resistance (e.g. extra connecting plates, gap recovering systems) which would unnecessarily increase the mesh complexity and the computational load in the FEM analyses. In SolidWorks, a special identifying prefix is then assigned to the geometric parameters, allowing

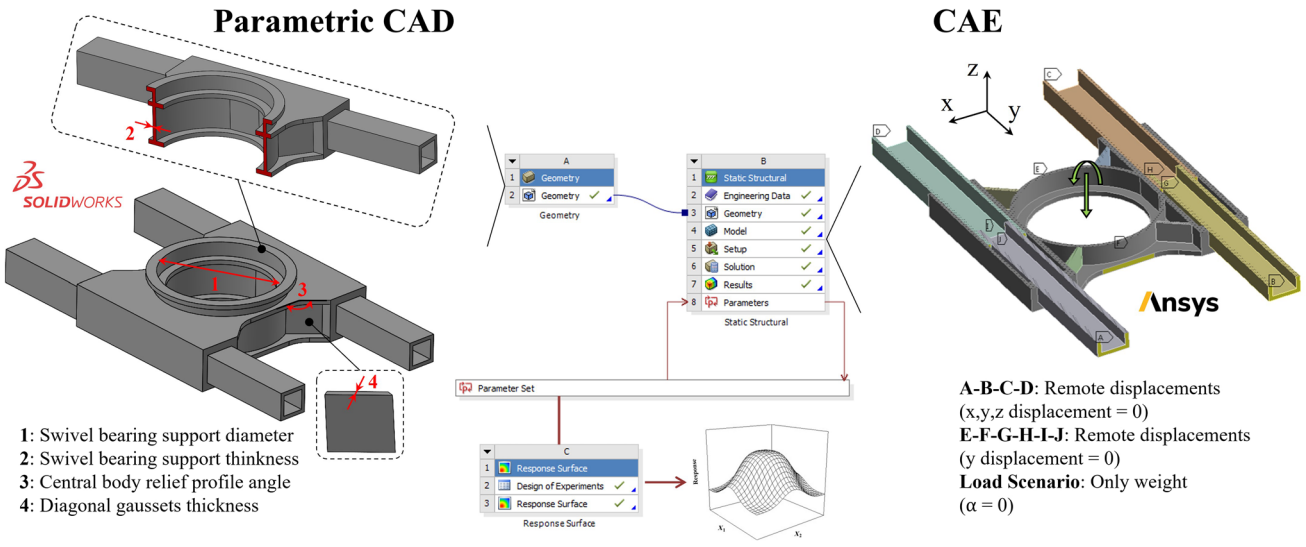

Fig. 12 CAD/CAE integrated framework: parametric CAD model and related CAE simulation setup

ANSYS to recognize and edit their values when required. The four geometric parameters considered in the study are the swivel bearing diameter and thickness, the central body relief profile angle, and the diagonal gaussets thickness, as illustrated in the left schematic of Fig. 12. Concerning the ANSYS model, shown in the right side of Fig. 12, the following conditions and settings are enforced:

- Linear isotropic elastic structural steel (elastic modulus, Poisson's ratio, and density set to 210,000 MPa, 0.33, and 7800 kg/m^3 respectively).
- Remote displacements ($x, y, z = 0$) at the extremities of the beams (i.e. regions A-B-C-D) to prevent rigid body motions, while rotations around x are left free.
- Additional remote displacement ($y = 0$) in I-J-H-G-E–F to consider the effect of the end stop pins;
- Purely frontal load ($\alpha = 0°$) applied on the swivel bearing support.
- Free mesh with second-order tethraedral elements (medium element size of 20 mm). A preliminary mesh convergence analysis has been conducted with both the simplified and the complete undercarriage geometries, by varying the element size from 15 to 40 mm. The obtained variations in terms of vertical displacement and bending stress are within 3%, indicating the model stability.
- Frictionless sliding contacts among the surfaces of the telescopic beam structure, adopting the pure-penalty formulation with auto-asymmetric behavior, trim tolerance of 1 mm and Gauss point detection.
- Nonlinear solver (NLGEOM option turned on) with 20 initial substeps, two minimum substeps, and 100 maximum substeps.
- Maximum vertical displacement registered at each simulation.

Under this setup, a single candidate is solved in about 15 min, whereas a complete undercarriage simulation model would take 2 to 4 h to converge. Even so, given that parametric studies involving four parameters can result in substantial number of samples for testing based on the chosen variation ranges and assigned levels for each parameter, time-saving measures are here implemented. In particular, to optimize efficiency, preminary studies are conducted to evaluate the impact of individual parameters on the overall bending behavior of the system.

From the preliminary analyses, two crucial parameters have been identified: the swivel bearing support diameter and the diagonal gaussets thickness (denoted as 1 and 4 respectively in Fig. 12). Subsequently, a two-dimensional parametric study comprising 20 simulations is conducted by varying these parameters within defined integer value spans (5 for the diameter, {990,1010,1030,1050,1080} mm and 4 for the thickness, {10,20,30,40} mm). The resulting vertical displacement map over the explored domain is presented in Fig. 13. Comparisons are then made between the FEM vertical displacement and the value obtained from the analytical model, which does not include the geometric parameters considered in the FEM analysis and, consequently, provides a uniform result for all cases. The numerical results, specifically 6.098 for FEM (average value) and 6.280 for the analytical model, indicate a difference of 12.4%. Consequently, a corrective coefficient of 1.124 has been applied to J_c in the analytical model.

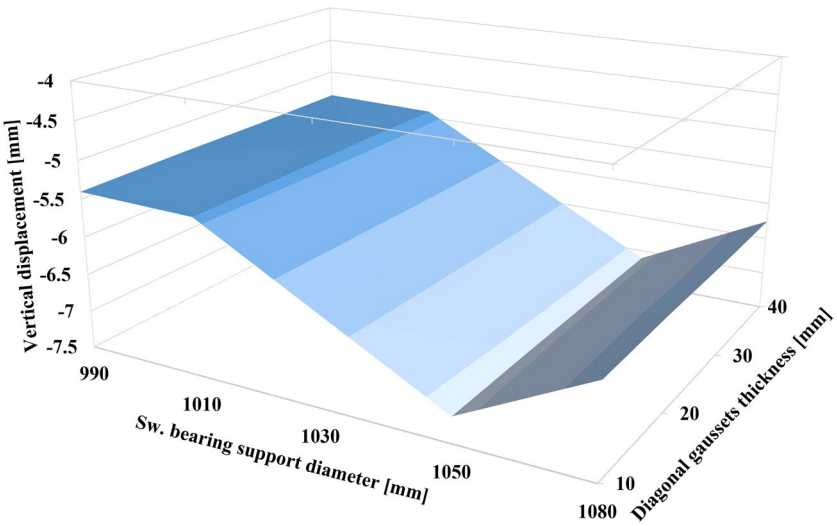

Fig. 13 Response surface of the maximum vertical FEM displacement for different geometric configurations

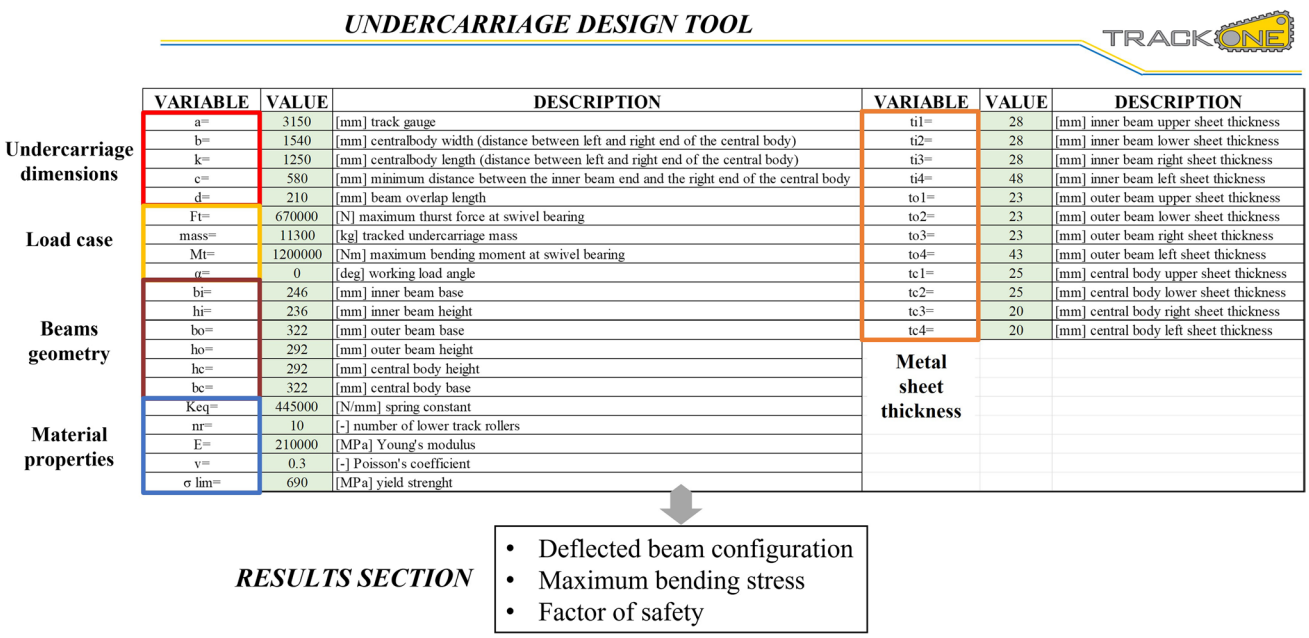

VARIABLE	VALUE	DESCRIPTION	VARIABLE	VALUE	DESCRIPTION
a=	3150	[mm] track gauge	ti1=	28	[mm] inner beam upper sheet thickness
b=	1540	[mm] centralbody width (distance between left and right end of the central body)	ti2=	28	[mm] inner beam lower sheet thickness
k=	1250	[mm] centralbody length (distance between left and right end of the central body)	ti3=	28	[mm] inner beam right sheet thickness
c=	580	[mm] minimum distance between the inner beam end and the right end of the central body	ti4=	48	[mm] inner beam left sheet thickness
d=	210	[mm] beam overlap length	to1=	23	[mm] outer beam upper sheet thickness
Ft=	670000	[N] maximum thurst force at swivel bearing	to2=	23	[mm] outer beam lower sheet thickness
mass=	11300	[kg] tracked undercarriage mass	to3=	23	[mm] outer beam right sheet thickness
Mt=	1200000	[Nm] maximum bending moment at swivel bearing	to4=	43	[mm] outer beam left sheet thickness
α=	0	[deg] working load angle	tc1=	25	[mm] central body upper sheet thickness
bi=	246	[mm] inner beam base	tc2=	25	[mm] central body lower sheet thickness
hi=	236	[mm] inner beam height	tc3=	20	[mm] central body right sheet thickness
bo=	322	[mm] outer beam base	tc4=	20	[mm] central body left sheet thickness
ho=	292	[mm] outer beam height			
hc=	292	[mm] central body height			
bc=	322	[mm] central body base			
Keq=	445000	[N/mm] spring constant			
nr=	10	[-] number of lower track rollers			
E=	210000	[MPa] Young's modulus			
ν=	0.3	[-] Poisson's coefficient			
σ lim=	690	[MPa] yield strenght			

Fig. 14 Industrial design tool

Table 1 Main characteristics of the tested undercarriages (U-1, U-2, and U-3)

Parameter	U-1	U-2	U-3
a[mm]	3150	3200	3800
Mass [kg]	7750	11,900	17,500
F_t[N]	390,500	560,000	751,000
M_t[Nm]	594,000	960,000	1,758,000

4 Model validation for interactive design tool

4.1 FEM validation

The derived analytical formulas, opportunely corrected as outlined in Section 3.4, have been integrated into an Excel spreadsheet, illustrated in Fig. 14. This has resulted in a precise and fast structural verification tool conceived for utilization in the early stages of undercarriage design, facilitating the evaluation of new prototypes. Users are prompted to input key undercarriage dimensions, beam geometry, material properties, and load case details. The interactive design tool generates outputs for the front axle vertical displacement and maximum stress values. By swiftly comparing this value with the stress limit of the chosen material, the tool also provides the factor of safety of the current design variant. This enables users to assess whether the values align with predetermined acceptability limits (displacement and stress) established during the preliminary phases of the design process and defined by company specifications.

To verify the tool correctness, three undercarriage models have been selected from the product catalog of the industrial partner [32] and subsequently tested. These are subject to the primary load scenarios, namely frontal ($\alpha = 0°$) and lateral ($\alpha = 90°$) loads. The proposed model and tool undergo validation against the FEM simulations of the complete undercarriage models. The considered parameter sets are listed in Table 1, whereas the main outputs of the analyses are presented in Fig. 15. Overall, the analytical and FEM plots match very well, with differences within 10% in almost all the examined cases, as visible in Table 2. The positive effects of the corrections made in Section 3.4 can also be seen from the results (see dotted lines in Fig. 15). The analytical model is less effective at capturing the local effects on the beams, which still require verification through FEM approaches. However, compared to standard FEM performed in ANSYS, the novel tool accurately captures the beam deflection and stress states while significantly reducing computational time. Notably, on a workstation with an Intel(R) Core (TM) CPU @ 2.5 GHz and 16 GB RAM, the total time to solve a single candidate is reduced by six orders of magnitude, dropping from 15,000 to 0.005 s. The high computational efficiency makes the analytical model highly suitable for conducting large optimization studies within a limited amount of time, as it will be shown in Section 4.2, reserving FEM for final checks on the best candidate.

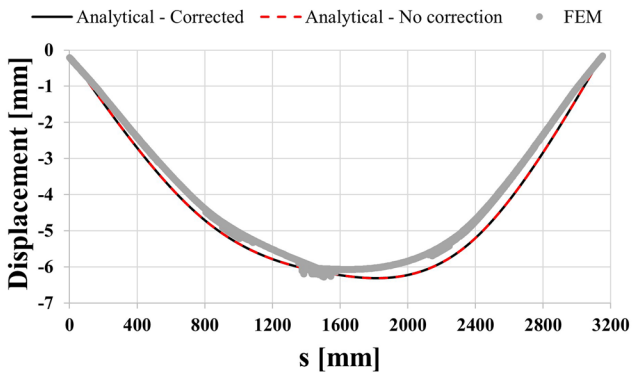

(a) U-1, α = 0°. Max stress: 175 MPa (Analytical) Vs. 169 MPa (FEM).

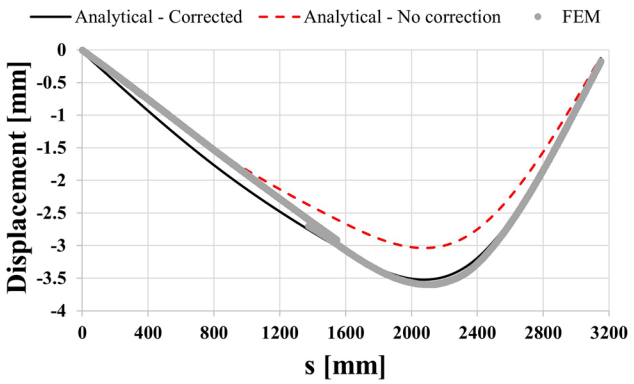

(b) U-1, α = 90°. Max stress: 149 MPa (Analytical) Vs. 151 MPa (FEM).

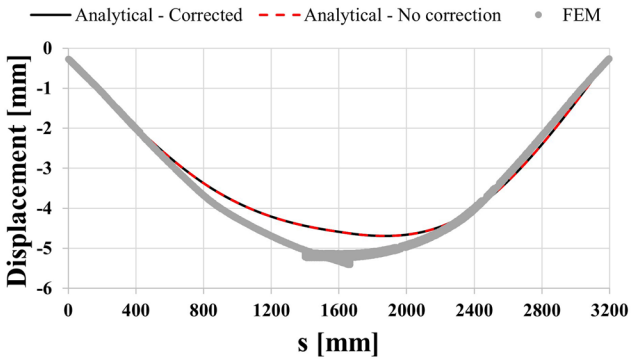

(c) U-2, α = 0°. Max stress: 142 MPa (Analytical) Vs. 125 MPa (FEM).

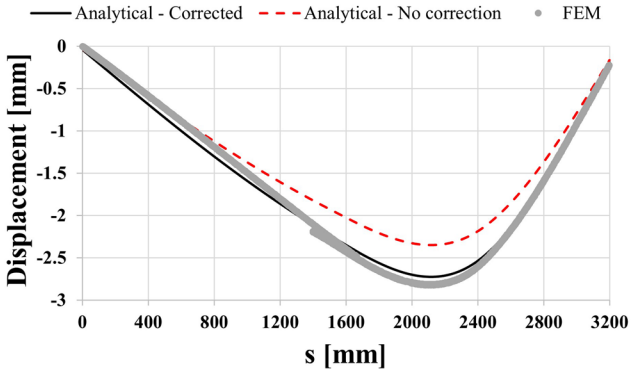

(d) U-2, α = 90°. Max stress: 125 MPa (Analytical) Vs. 123 MPa (FEM).

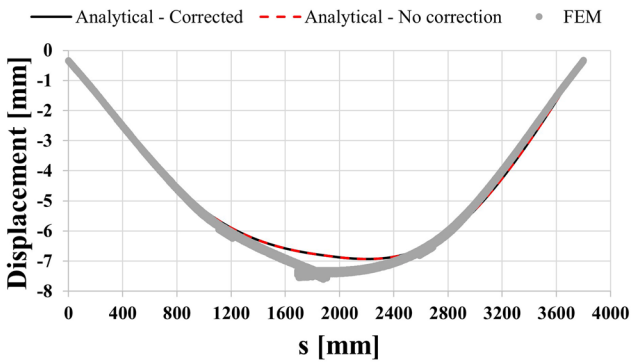

(e) U-3, α = 0°. Max stress: 182 MPa (Analytical) Vs. 174 MPa (FEM).

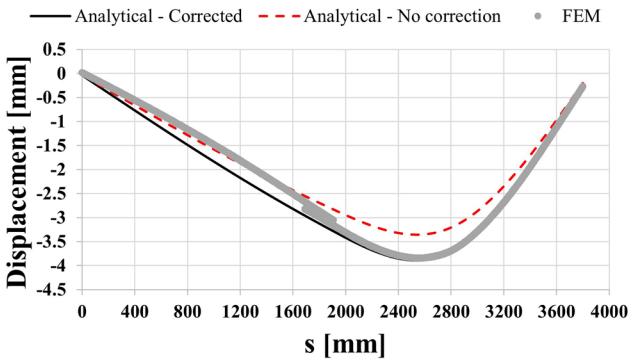

(f) U-3, α = 90°. Max stress: 158 MPa (Analytical) Vs. 152 MPa (FEM).

Fig. 15 Model validation results

Table 2 Errors in result comparisons: U_z error is presented as both an average (Avg) across the entire beam length ($s \in [0, a]$) and specifically at the most critical beam section, where also stress value is taken

	Error [%]					
	U-1 $\alpha = 0°$	U-1 $\alpha = 90°$	U-2 $\alpha = 0°$	U-2 $\alpha = 90°$	U-3 $\alpha = 0°$	U-3 $\alpha = 90°$
U_z	10.3 (Avg) 10.2 (s=2355mm)	8.2 (Avg) 2.7 (s=2355mm)	7.4 (Avg) 1.0 (s=2395mm)	3.0 (Avg) 2.7 (s=2395mm)	3.9 (Avg) 2.2 (s=2835mm)	11.8 (Avg) 0.8 (s=2835mm)
$\sigma_{b,max}$	3.6	1.3	13.6	1.6	4.6	3.9

Table 3 Numerical results of the optimization study

Objective function	Design variables				Constraints				
h_o[mm]	b_i[mm]	h_i[mm]	t_o[mm]	t_i[mm]	$U_{z,max}$[mm]	$\sigma_{b,max}$[MPa]	b_i/h_i	b_o/h_o	t_i/t_o
300	490	250	25	50	11.21	199.20	1.96	1.80	2.00

4.2 Design optimization study

To show the benefits of incorporating well-tuned analytical models into the preliminary design phases of commercial undercarriages, a size optimization study is conducted in this section [36, 39, 40]. Adopting as a test case the U-3 prototype reported in Table 2, the aim is to find the best set of plate thicknesses ($t_{i,j}$, being $i = \mathrm{o,i,c}$ and $j = 1,2,3,4$ as reported in Section 3.3) and inner beam dimensions (b_i and h_i) which minimizes the height of the outer beam (h_o). In fact, according to the industrial practice, reducing the vertical profile of the undercarriage telescopic beam system would yield significant advantages for the design of the upper machine, as typically requested by the client. Adopting a uniform thickness for all beams (i.e. $t_1 = t_2 = t_3 = t_4$) to facilitate manufacturing, the size optimization problem may be formalized as follows:

$$\textbf{Minimize } h_o \tag{51}$$

$$\textbf{Constraints} \rightarrow \begin{cases} U_z(s) \leq U_{z,lim} \\ \sigma_b(s) \leq \sigma_{b,lim} \\ b_i/h_i \leq \varepsilon \\ b_o/h_o \leq \varepsilon \\ t_i/t_o \leq \varepsilon \end{cases} \tag{52}$$

$$\textbf{Design variables} \rightarrow \begin{cases} b_i = \{60,65,70,\ldots,595,600\}mm \\ h_i = \{60,65,70,\ldots,595,600\}mm \\ t_o = \{5,6,8,10,12,15,16,20,25,30,35,40,45,50,55,60\}mm \\ t_i = \{5,6,8,10,12,15,16,20,25,30,35,40,45,50,55,60\}mm \end{cases} \tag{53}$$

The imposed constraints ensure acceptable deflection values, preserve the structural integrity of the multi-beam system, and maintain correct proportions among the beams. Specifically, the limit for vertical displacement $U_{z,lim}$, bending stress $\sigma_{b,lim}$ and the shape factor ε are set to 15 mm, 200 MPa (providing a safety factor of ≈1.8 for standard S355 steel), and 2, respectively. Concerning the design variables, their values are varied within the specified intervals based on the commercially available sizes of metal sheets in the market. The size optimization problem has been solved using the *intlinprog* routine in Matlab. The convergence has been reached after 600,000 iterations with a total elapsed time of approximately 50 min. The results of the study are summarized in Table 3.

The optimized dimensions lead to a reduction of the outer height h_o by approximately 12.3%, i.e. decreasing from the original 342 mm (used in the current commercial U-3 undercarriage) to 300 mm, while still meeting all prescribed performance requirements. Implementing this study in FEM software, e.g. utilizing the framework proposed in Fig. 12, would either necessitate significant model simplifications or result in excessive computational times.

4.3 Tool integration into design workflow

The proposed tool seamlessly integrates into the dimensioning and structural phases of the workflow outlined in Fig. 3, primarily boosting the design and size optimization of novel custom solutions and therefore contributing in terms of company competitiveness. Furthermore, relevant benefits can be seen also from the manufacturing standpoint. In particular, the reported approach facilitates the development of technical solutions that utilize standard plates thicknesses and predefined maximum overall dimensions of the beam structure, as discussed in Section 4.2. The use of standard plate thicknesses enables the suppliers to gather material more quickly and reduces the frame cost. It also enhances the efficiency of metal sheet cutting, improves nesting, and reduces waste. Ideally, the design can be pushed to the point where the beam dimensions (base-height) are the ones typical of commercial profiled rectangular bars, making the welding not necessary. On the other hand, by adhering to predefined dimensions, the beam length can be minimized, resulting in reduced material machining during production and mitigating distortions caused by welding thermal alterations.

5 Conclusions

This work proposes a novel method and tool to synthesize tracked undercarriages with extendable telescopic beams of any class and weight. The novel design tool, which promptly provides the undercarriage vertical displacement and bending stress in significantly shorter timeframes compared to standard FEM, is based on a theoretical model defined starting from an in-depth analysis of the telescopic beams geometry in a CAD

environment and from preliminary CAE results. The 3D structural problem has been simplified by modeling a schematic geometry and deriving loads for the front axle of the undercarriage, resulting in a planar multi-beam system. Afterwards, the model has been refined through the incorporation of corrective coefficients aimed at minimizing output errors. Parametric studies have been conducted via an integrated CAD/CAE simulation environment to evaluate the correction to be applied for the geometric and load simplifications introduced in the modeling of the central body. In particular, a multi-software framework consisting of SolidWorks and ANSYS Workbench has been defined to rapidly assess the influence of the main geometric parameters of the central body on its structural properties. The tool has been validated against FEM data for three undercarriage models from the industry repository, demonstrating a strong correlation with maximum errors within the 10% for the majority of the cases. At last, a size optimization study has been carried out in Matlab to reduce the outer beam height and favor the design and assembly of the upper machine. The proposed tool converged to a feasible solution and successfully demonstrated its suitability for managing multi-variable optimization studies. Its higher computational efficiency enables extensive comparative analyses, facilitating the standardization of beam structures across various undercarriage configurations. This optimization strategy allows to reduce the number of components in the bill of materials, simplifying manufacturing and welding processes.

Author contribution All authors contributed to the study conception and design. Material preparation, data collection, and analysis were performed by Luca Catenacci and Andrea Cavedoni. The first draft of the manuscript was written by Pietro Bilancia and Marcello Pellicciari, and all authors commented on previous versions of the manuscript.

Funding Open access funding provided by Università degli Studi di Modena e Reggio Emilia within the CRUI-CARE Agreement.

Data availability A folder containing the research data and the Matlab scripts with analytical formulas related to this work will be made available upon request to the Authors.

Declarations

Conflict of interest The authors declare no competing interests.

References

1. Zhong RY, Xu X, Klotz E, Newman ST (2017) Intelligent manufacturing in the context of industry 4.0: a review. Engineering 3:616–630. https://doi.org/10.1016/J.ENG.2017.05.015
2. Dudziiqski PA (1989) Design characteristics of steering systems for mobile wheeled earthmoving equipment. J Terramech 26:25–82. https://doi.org/10.1016/0022-4898(89)90025-6
3. He R, Sandu C, Khan AK et al (2019) Review of terramechanics models and their applicability to real-time applications. J Terramech 81:3–22. https://doi.org/10.1016/j.jterra.2018.04.003
4. Muro T (1982) Tyres/Wheels and tracks state-of-the-art report. J Terramech 19:55–69
5. Vondráčková T, Voštová V (2017) Selection of excavators for earth work on the basis of their performance. In: IOP Conf. Ser.: Mater Sci Eng 245 022086. https://doi.org/10.1088/1757-899X/245/2/022086
6. Dwyer MJ, Okellot JA, Scarlettt AJ (1993) A theoretical and experimental investigation of rubber tracks for agriculture. J Terramech 30:285–298. https://doi.org/10.1016/0022-4898(93)90016-Q
7. Dadhich S (2015) A survey in automation of earth-moving machines. Luleå tekniska universitet, Luleå. Available from: https://urn.kb.se/resolve?urn=urn:nbn:se:ltu:diva-21987
8. Zhu X, Pan L, Sun Z et al (2022) Simulation tool for dozer data acquisition. Autom Constr 142. https://doi.org/10.1016/j.autcon.2022.104522
9. Erbach DC (1994) Benefits of tracked vehicles in crop production. Dev Agric Eng 11:501–520
10. Vu MT, Choi HS, Kim JY, Tran NH (2016) A study on an underwater tracked vehicle with a ladder trencher. Ocean Eng 127:90–102. https://doi.org/10.1016/j.oceaneng.2016.09.036
11. Wang M, Wu C, Ge T et al (2016) Modeling, calibration and validation of tractive performance for seafloor tracked trencher. J Terramech 66:13–25. https://doi.org/10.1016/j.jterra.2016.03.001
12. Nazaruddin, Kiki, Gunawan (2015) Undercarriage design of excavator model in application of various track drive. J Subsea and Offshore 26:1–6.
13. Liao KW, Ha C (2008) Application of reliability-based optimization to earth-moving machine: hydraulic cylinder components design process. Struct Multidiscip Optim 36:523–536. https://doi.org/10.1007/s00158-007-0187-2
14. Xie X, Han X, Zhang Z et al (2023) Structural design and test of arch waist dynamic chassis for hilly and mountainous areas. Int J Adv Manuf Technol 127:1921–1933. https://doi.org/10.1007/s00170-022-10224-0
15. Chen Z, Wen G, Wang H et al (2022) Multi-resolution nonlinear topology optimization with enhanced computational efficiency and convergence. Acta Mechanica Sinica/Lixue Xuebao 38. https://doi.org/10.1007/s10409-021-09028-x
16. Liu J, Wen G, Xie YM (2016) Layout optimization of continuum structures considering the probabilistic and fuzzy directional uncertainty of applied loads based on the cloud model. Struct Multidiscip Optim 53:81–100. https://doi.org/10.1007/s00158-015-1334-9
17. Bilancia P, Berselli G (2021) an overview of procedures and tools for designing nonstandard beam-based compliant mechanisms. CAD Comput Aided Des 134. https://doi.org/10.1016/j.cad.2021.103001
18. Reece~ AR (1984) A rational approach to the design of earth-moving machines*
19. Welling O, Shoop S, Letcher T et al (2022) Estimation of plowing forces on vehicles driving through deep snow. J Terramech 104:25–29. https://doi.org/10.1016/j.jterra.2022.08.003

20. Zhu W, Fan X, Tian L, He Q (2018) An integrated simulation method for product design based on part semantic model. Int J Adv Manuf Technol 96:3821–3841. https://doi.org/10.1007/s00170-018-1808-1
21. Dudziński PA, Chołodowski J (2021) A method for predicting the internal motion resistance of rubber-tracked undercarriages, Pt. 1. A review of the state-of-the-art methods for modeling the internal resistance of tracked vehicles. J Terramech 96:81–100
22. Chołodowski J, Dudziński PA (2021) A method for predicting the internal motion resistance of rubber-tracked undercarriages, Pt. 2. A research on the motion resistance of road wheels. J Terramech 96:101–115. https://doi.org/10.1016/j.jterra.2021.02.005
23. Chołodowski J, Dudziński PA, Ketting M (2021) A method for predicting the internal motion resistance of rubber-tracked undercarriages, Pt. 3. A research on bending resistance of rubber tracks. J Terramech 97:71–103. https://doi.org/10.1016/j.jterra.2021.06.001
24. Chen Z, Xue D, Wang G et al (2021) Simulation and optimization of the tracked chassis performance of electric shovel based on DEM-MBD. Powder Technol 390:428–441. https://doi.org/10.1016/j.powtec.2021.05.085
25. Gholami J, Ghassabi M (2021) Optimization and numerical investigation of an excavator carrier. J Terramech 97:29–34. https://doi.org/10.1016/j.jterra.2021.05.002
26. Taratorkin A, Derzhanskii V, Abdulov S, Taratorkin A (2022) Off-design loading modes of the road rollers of the undercarriage of the tracked vehicle. In: AIP Conference Proceedings 2503:080016. https://doi.org/10.1063/5.0099502
27. Bilancia P, Berselli G, Scarcia U, Palli G (2018) Design of a beam-based variable stiffness actuator via shape optimization in a CAD/CAE environment. In: ASME Smart Materials, Adaptive Structures and Intelligent Systems (Vol. 51944, p. V001T03A013). https://doi.org/10.1115/SMASIS2018-8053
28. Pehrson NA, Bilancia P, Magleby S, Howell L (2020) Load-displacement characterization in three degrees-of-freedom for general lamina emergent torsion arrays. Journal of Mechanical Design 142. https://doi.org/10.1115/1.4046072
29. Peng L, Liu L, Long T, Yang W (2014) An efficient truss structure optimization framework based on CAD/CAE integration and sequential radial basis function metamodel. Struct Multidiscip Optim 50:329–346. https://doi.org/10.1007/s00158-014-1050-x
30. Wang D, Hu F, Ma Z et al (2014) A CAD/CAE integrated framework for structural design optimization using sequential approximation optimization. Adv Eng Softw 76:56–68. https://doi.org/10.1016/j.advengsoft.2014.05.007
31. Wang J, Niu W, Ma Y et al (2017) A CAD/CAE-integrated structural design framework for machine tools. Int J Adv Manuf Technol 91:545–568. https://doi.org/10.1007/s00170-016-9721-y
32. TrackOne S.r.l. Product portfolio. https://www.trackone.it/en/products/. Accessed 18 Jan 2024
33. Pahl G, Beitz F, Jörg G, Karl-Heinrich (2007) Engineering design, 3rd edn. Springer, London
34. Shriyan G, Kshirsagar VV (2019) Modeling tracked vehicle to determine undercarriage performance. SAE Technical Paper 2019-28-0116. https://doi.org/10.4271/2019-28-0116
35. Yang X, Wen G, Jian L et al (2024) Archimedean spiral channel-based acoustic metasurfaces suppressing wide-band low-frequency noise at a deep subwavelength. Mater Des 238. https://doi.org/10.1016/j.matdes.2024.112703
36. Liu J, Ou H, Zeng R et al (2019) Fabrication, dynamic properties and multi-objective optimization of a metal origami tube with Miura sheets. Thin-Walled Structures 144. https://doi.org/10.1016/j.tws.2019.106352
37. Liu J, Chen T, Zhang Y et al (2019) On sound insulation of pyramidal lattice sandwich structure. Compos Struct 208:385–394. https://doi.org/10.1016/j.compstruct.2018.10.013
38. Bauchau OA, Craig JI (2009) Structural analysis: with applications to aerospace structures. Springer Science & Business Media (Vol 163). https://doi.org/10.1007/978-90-481-2516-6
39. Park HS, Dang XP (2010) Structural optimization based on CAD-CAE integration and metamodeling techniques. CAD Comput Aided Des 42:889–902. https://doi.org/10.1016/j.cad.2010.06.003
40. Cavazzuti M (2013) Optimization methods: from theory to design scientific and technological aspects in mechanics. Springer, Berlin Heidelberg